Analysis of Antenna Impact on Wide-Band Indoor Radio Channel and Measurement Results at 1 GHz, 5.5 GHz, 10 GHz and 18 GHz

Giovanni Santella

Abstract: **The object of this paper is to investigate the influence of antenna pattern on indoor radio channel characteristics. Different from previous works where this analysis was carried out at a fixed frequency using different antennas, in the present paper (where measurements were taken in a wide frequency range) the variation of the radiation pattern was caused by two factors: the change of the radiation pattern when the same antenna was used at different frequencies and the use of different type of antennas. To carry out this analysis, frequency domain measurements of the indoor radio channel at 1 GHz, 5.5 GHz, 10 GHz and 18 GHz were collected. Measurements were taken using a network analyzer. Several realizations of the channel transfer function were obtained varying, for each measurement, the position of the transmitter and keeping the receiver fixed. Estimate of the channel impulse response was obtained from the Inverse Fourier Transform (IFT) of the frequency response. The measurements were performed in an office environment with mostly metallic walls and inner separations. The obtained data were elaborated to obtain the power versus distance relationship, the Cumulative Distribution Functions (CDFs) of rms Delay Spread (DS) and of the 3 dB frequency correlation bandwidth. Finally, the 3 dB width of the frequency correlation function has been empirically related to the inverse of the rms DS of the impulse response.**

Index Terms: **Indoor channel, wide-band measurements.**

I. INTRODUCTION

The increased interest in high bit rate radio links within buildings has recently renewed the attention paid to wide-band measurements of the indoor radio channel. As an example today there is a growing need for indoor wireless communications, such as wireless local area network (WLAN) systems, to provide high-speed digital transmission between computer terminals. WLANs have attractive features such as their layout flexibility and terminal portability. WLANs at 2.4 GHz and 19 GHz are currently is use in Japan [1] with data rates compatible with that of the wired -Ethernet system (10 Mbps). However, the data rate of future indoor wireless networks is expected to reach as high as 156 Mbps.

Due to spectrum crowding at UHF and frequency reuse limits in adjacent cells, particularly attractive is the 18-19 GHz band [2]. Another advantage in using higher frequencies is that more compact and directive antennas can be used. Omnidirectional transmission in the azimuth plane can be obtained using intelligent Six-Sector Microwave antennas as suggested in [2], [3]. Wide-band measurements of the indoor radio channel have been performed both in the time domain [4]–[10], [27] and frequency domain [11]–[18], [26], [28]. Today however, there are few propagation results available in the literature which compare indoor radio channel characteristics in different bands [5], [15], [16], [20], [21], [26], [28].

The radio channel characteristic is generally strongly influenced by the antenna radiation pattern and polarization. Up to now, little attention has been paid to this issue. An interesting analysis of this problem has been carried out in [27] where indoor wide band measurements have been carried out at a fixed frequency (2.45 GHz) but varying antenna polarization and directivity. In particular, twenty-five different TX-RX antenna combinations were considered. The measurement results obtained in [27] point out a significant influence of the radiation pattern on the delay spread and maximum excess delay (MED: is the maximum excess delay at which an echo is received with amplitude 10 dB down from maximum signal level). The object of this paper is to investigate on the influence of antenna pattern on indoor radio channel characteristics. The idea behind this work was that of analysing what happens when we move towards higher frequencies taking into account that usually we tend to use more directive antennas in order to increase the transmitter power. Different from [27], where this analysis was carried out at a fixed frequency using different antennas, in the present paper (where measurements were taken in a wide frequency range) the variation of the radiation pattern was caused by two factors: the change of the radiation pattern when the same antenna was used at different frequencies and the use of different type of antennas at different frequencies. In the present work, coherent frequency-domain wideband propagation measurements of a indoor radio channel have been taken at 1 GHz, 5.5 GHz, 10 GHz and 18 GHz. At 1 GHz, 5 GHz and 10 GHz two discone antennas with similar radiation patterns were adopted. However their directivity in the vertical plane showed an increase with frequency. At 18 GHz a directive horn antenna was adopted at the receiver and a bi-conical antenna at the transmitter. Thus, the radiation patterns showed different characteristics at the different frequencies investigated. Estimate of the time-domain response from the frequency domain measurements is obtained by taking the IFT of the measured data. Statistical behavior of the measurement results is compar-

Manuscript received February 9, 1999; approved for publication by Henry Bertoni, Division II Editor, September 18, 1999.

G. Santella is with Fondazione Ugo Bordoni, Viale Europa 190, 00144, Rome, Italy, e-mail: gianni@fub.it.

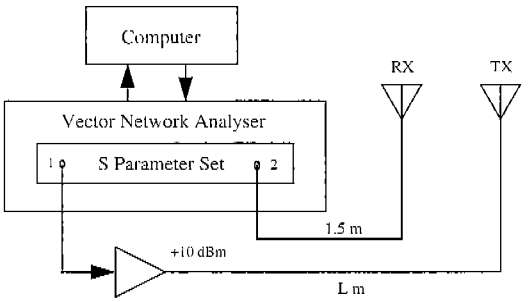

Fig. 1. Block diagram of the swept-frequency measurement system.

ed at the different frequencies considered.

The remainder of this paper is organized as follows: in Section II the measurement system and the investigated indoor environment are described; in Section III the results of the analysis of the collected measurement data are reported; in Section IV the obtained results are explained using a simple indoor propagation model; conclusive considerations are given in Section V.

II. MEASUREMENT SYSTEM

The frequency domain measurements of the indoor channel carried out in the present work are obtained using the system shown in Fig. 1.

The measurement set up includes a network analyzer whose output is a 10 dBm RF signal. This equipment is connected to the transmitting antenna by a low loss cable Lm long (L varies according to the dimension of the area to be measured).

The measured data are read and stored by a PC. The channel transfer function is sampled at the following frequencies:

$$f_i = f_0 + (i - 201)f_s\,, \qquad i = 1, \ldots, 401, \qquad (1)$$

where f_0 is the central frequency of the band sounded, f_s = 1 MHz is the frequency step between adjacent samples. The resulting aliasing-free range in the time domain is therefore 1 μs. The sweep time is 400ms. The vector network analyzer was calibrated connecting the two cables to each other (without the TX and RX antennas) and starting the automatic calibration procedure. In this way the linear distortion introduced by the cables is removed from the measurement results. The bandwidth of the channel transfer function analyzed is 400 MHz which corresponds to a resolution of 2.5 ns in the time domain. An example of magnitude (dB) and phase (degree) of indoor channel frequency response is reported in Fig. 2 for line of sight (LOS) condition. The time domain impulse response obtained by taking the IFT of the frequency response is also shown in Fig. 2. The presence of echoes is clearly visible on the impulse response while deep magnitude nulls and abrupt phase changes can be observed on the frequency response .

Windowing is applied to the frequency response before using IFT to obtain the time response, as suggested in [11], [12].

It should be noted that the impulse response of the indoor radio channel is greatly influenced by the type of transmitting and receiving antennas used [14], [18], [27]. Thus, antennas have to be regarded as a part of the indoor radio channel. For the experiments at 1 GHz, 5.5 GHz and 10 GHz, two discone

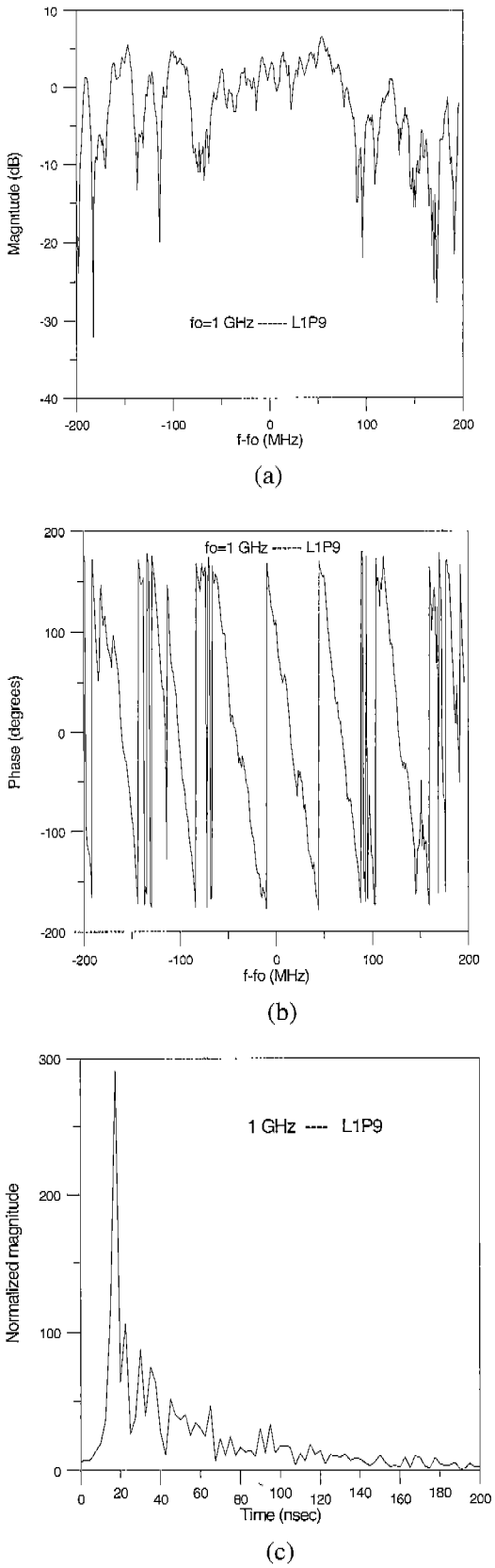

Fig. 2. An example of a measurement made with the network analyzer: (a) The magnitude of the frequency response in decibels, (b) the phase of the frequency response in degrees, and (c) the magnitude of the IFT of the frequency response.

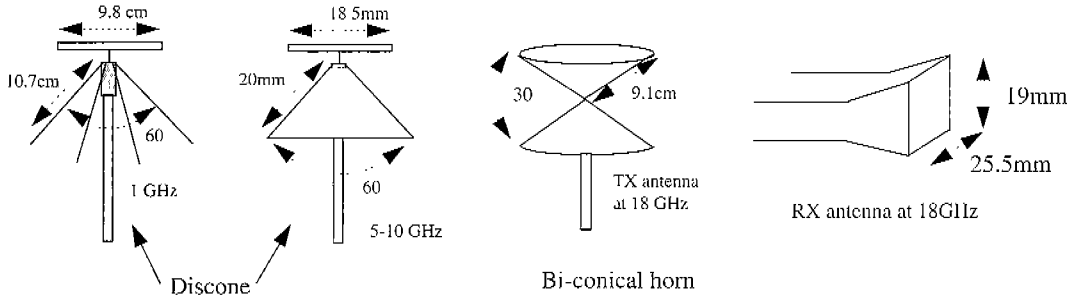

Fig. 3. Schematic representation of antennas adopted during the experiments.

type antennas were used for transmission and reception. These antennas exhibit an omnidirectional radiation pattern in the azimuth plane, an approximately eight-shaped beam in the elevation plane, vertical polarization and about 2 dB directivity. For the present experiment, two different discone antenna pairs were built: the first pair was used for the measurements at 1 GHz, the second pair was used at 5 GHz and 10 GHz (see Fig. 3). The 3 dB elevation beamwidth of the discone antenna adopted at 1 GHz is 80°. The second discone adopted at 5.5 GHz shows similar radiation characteristics as the discone used at 1 GHz but narrower vertical beamwidth, while at 10 GHz its 3 dB elevation beamwidth reduces to about 50° and the direction of maximum directivity is tilted downwards of about 35°. A discone antenna was preferred to a $\lambda/4$ dipole due to its larger bandwidth. This fact was important at 1 GHz where the band sounded constituted 40 % of the central frequency. For the experiments at 17.5 GHz, a directional horn antenna was used at the receiver site (its directivity is about 12 dB, the 3 dB beamwidth in the azimuth plane is 40° and the polarization is vertical) and a bi-conical horn antenna at the transmitter. Bi-conical horn antenna is still omnidirectional in the azimuth plane with a directivity of about 4 dB. More details on discone and bi-conical horn antennas adopted can be found in [22], [23], and Appendices A and B.

A. Measurement Procedure

Measurements were carried out in the indoor environment shown in Fig. 4 where, as indicated, rooms are delimited mostly by smooth metallic walls. The height of the ceiling is 4m. Just a few small objects were present in the room in order to reduce the clutter. It has to be noted that metallic walls do not represent the majority of indoor environments. Two interior separations are made by glass windows encased in a steel frame. One of the sides consists of large glass windows in a steel frame, from 1m height to the ceiling, and concrete beneath. Metallic chairs and wooden tables with metallic legs were present in the rooms. Measurements with both LOS and obstructed sight (OBS) situations were collected. Measurements were taken, for each frequency, in the positions corresponding to the intersections of the grid indicated by dotted lines. This resulted in about 60 impulse response outcomes for each experiment. For data gathering, these points were denoted as L"i"P"j" with i = 1,....5, j=1,...,15. As an example, measurements shown in Fig. 2 was taken at position L1P9. During the experiment, the transmitting antenna was moved while the receiving one was kept fixed. To

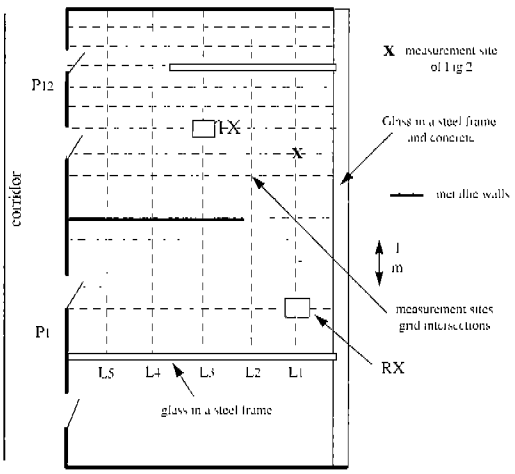

Fig. 4. Measurement site layout.

investigate on the effect of antenna height on channel characteristics, the transmitting antenna was located at 1.5m and 2.5m above the floor, in different experiments. The receiving antenna was always kept at 1.5m height. During the measurements, people stopped moving to avoid time variations of the channel during the measurement.

III. ANALYSIS OF THE MEASUREMENT RESULTS

In this section the experimental relationship between received power and distance is determined. In addition, the statistics of the rms DS and of the 3 dB width of the frequency autocorrelation function are derived and an empirical relationship between them is investigated (similar studies are reported in [4]–[12], [28]).

A. Power-Distance Relationship

The wideband normalized average received power (P_r) at any location x is [11]

$$\frac{P_r(x)}{P_t} = \frac{1}{N}\sum_{i=1}^{N} |H(f_i, x)|^2 , \qquad (2)$$

where P_t is the transmitted power, constant throughout the measured bandwidth, N is the number of samples of the frequency domain and $H(f_i, x)$ is the frequency response at frequency

f_i. For the power-distance relationship, the following model is adopted:

$$P_r(d) = Ad^{-\alpha}, \tag{3}$$

where d is the distance from the transmitter, α is the exponent of the power-distance relationship and A is a constant which depends on the transmitted power and the measurement system gain. Eq.(3) is often presented in logarithm form:

$$10\log_{10}[P_r(d)] = 10\log_{10}[A] - 10\alpha\log_{10}(d). \tag{4}$$

Most of the α values reported for office environments vary from 2(free space value) to 3, but lower and higher values have been reported for other indoor environments [1]–[20], [28].

As an example, in [11] values between 2.2 and 2.6 were found at 1 GHz; in [12] the α values were between 2.46 and 2.6 at 1 GHz; in [14], where 60 GHz measurements were carried out, values of α close to zero for both LOS and OBS situations were mostly observed. This fact was attributed to the combination effect of path loss and antenna gain compensation. In [16], α was found to be (LOS case) 1.5, 1.7, 1.6 at respectively 2 GHz, 5 GHz and 17 GHz. In [24] the path loss exponent values estimated range between 1.6 and 2.4 varying with the wall's material and frequency. In [26] the values for the path-loss law exponent found for LOS paths are within the range 1.8-2.0 for all frequencies (2.4 GHz, 4.75 GHz, 11.5 GHz). In OBS situations the loss law exponent increases with frequency and its value is 3.3, 3.8, and 4.5 at 2.4 GHz, 4.75 GHz, and 11.5 GHz, respectively. In [28] measurements were taken in the frequency domain at 2 GHz, 5 GHz and 17 GHz. Here, the transmit and receive antennas were both bi-conical omnidirectional and the sweep bandwidth was 500 MHz (corresponding to a time domain resolution of 2 ns). The values for the path-loss law exponent found in [28] for LOS paths range between 1.56 and 1.98 in the whole frequency range.

In the experiment whose results are presented in this paper, the average normalized received power was estimated, for each frequency response, using (2). Then, by linear regression analysis, the minimum mean square error (MMSE) line provides the dependence of the average received power (dB) on $10\log_{10}$ of distance. The slope of the regression line gives the experimental value of α. The measurement points that have been considered are only for LOS condition and correspond to the column L1 of Fig. 4 (12 points with 0.5m step size). A scatter plot on a log scale of the normalized received power versus the separation distance for LOS measurement situations is shown in Fig. 5 at different frequencies and with transmitter placed at 1.5m and 2.5m heights. Before proceeding it is worthwhile underlining that apparently the received power results at 18 GHz show lower path loss than those at 5 and 10 GHz. However this result can be easily explained if the antennas adopted in this experiment are considered (see Section II). In fact, in the experiments at 1 GHz, 5 GHz and 10 GHz the antennas adopted were omnidirectional in the azimuth plane both at the transmitter and receiver (about 2 dB gain). In the experiment at 18 GHz instead, the receiving antenna was directive with about 12 dB of gain and during the measurements the receiver horn was always pointed towards the

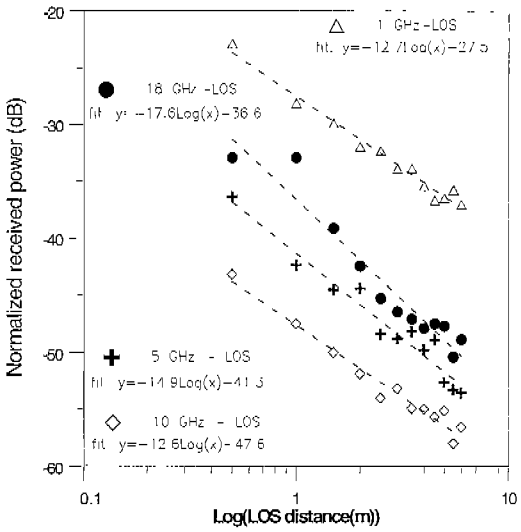

(a)

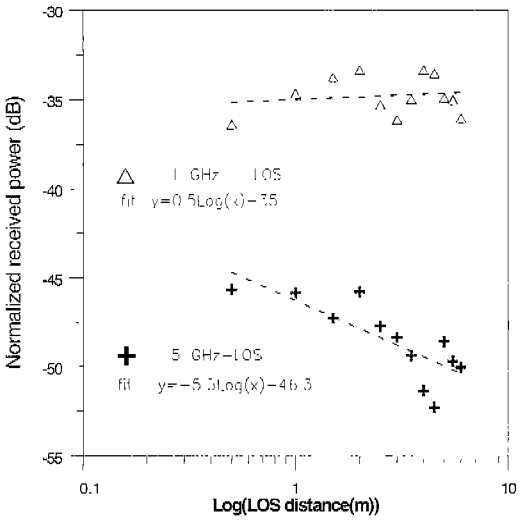

(b)

Fig. 5. Scatter plot and MMSE of the normalized received power (dB) versus the distance at different frequencies and in LOS condition: (a) TX antenna height = 1.5m, RX antenna height = 1.5m, (b) TX antenna height = 2.5m, RX antenna height = 1.5m.

open part of the metallic wall shown in Fig. 4 (that is the direction of arrival of the electromagnetic energy). The values of α obtained by linear regression analysis of data are reported in Table 1. These values show that in the case both TX and RX antennas were at 1.5m height, α values range between 1.26 and 1.76 (showing no clear trend with frequency increase) whereas, when the TX antenna is raised to 2.5m, measured values of α approaches to zero. This latest effect, pointed out also in [14], is due to the fact that the antenna gain compensates for path loss, as depicted in Fig. 6, obtaining an almost uniform pico-cell coverage. In fact, if a remote radio terminal is located in the vicinity of the base station (BS) antenna, such as RS1, the direct ray experiences both low path loss and small antenna gain. The contrary happens for the distant receiver RS2. However it has to be underlined that although uniform coverage is obtained, this coverage is poor. In fact if Figs. 5(a) and (b) results are compared, it can be observed that, at 1 GHz, Fig. 5(a) shows an attenua-

Table 1. Experimental α values.

Freq.(GHz)/ TX height(m)	1	5.5	10	18
1.5	1.27	1.45	1.26	1.76
2.5	-0.05	0.53	*	*

* not reliable data due to low signal to noise ratio.

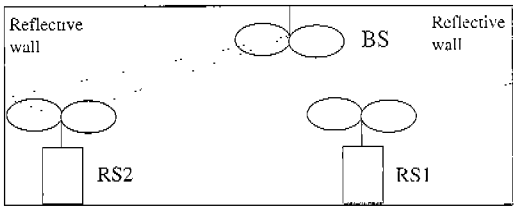

Fig. 6. Lay out of indoor radio network.

tion that ranges between -22 dB and -35 dB while in Fig. 5(b) it is, for the same frequency, constant at around -35 dB. Likewise, the 5 GHz curve of Fig. 5(a) shows an attenuation value between -36 dB and -52 dB while in Fig. 5(b) it is between -45 dB and -54 dB, for the same frequency. Fig. 5 also shows irregular variations of received power values versus distance. This is the result of constructive and destructive addition of different path contributions which add at the receiver site.

B. The rms Delay Spread

The rms DS , τ_{rms} , is defined as [11], [12]

$$\tau_{rms} \equiv \sqrt{\overline{\tau^2} - (\bar{\tau})^2}\,, \tag{5}$$

where

$$\overline{\tau^n} \equiv \frac{\sum\limits_k \tau_k^n \left|h(\tau_k, x)\right|^2}{\sum\limits_k \left|h(\tau_k, x)\right|^2}\,, \qquad n = 1, 2\,. \tag{6}$$

$h(t, x)$ is the measured time domain response and τ_k's are delays at which peak values of the time response indicate the arrival of the paths.

In this experiment $h(t, x)$ is obtained from the IFT of the measured frequency response. Windowing, applied in the frequency domain, causes sidelobes in the time domain response whose magnitude depends on the window type [11], [12] (for example rectangular and Hamming windows have sidelobes that are 13 dB and 41 dB down from the mainlobe, respectively). A comparison of delay spread values in different frequency bands has been carried out in some papers and some significant results are in the following reported. In [5], for instance, the results of propagation experiments in the 600 MHz and 1.7 GHz radio frequency bands have been reported. A slight difference in rms DSs in the two frequency bands was found without any trend with frequency, while the standard deviation of rms DS was greater for the measurement results in the 1.7 GHz band. In [20], where delay spread and signal level measurements were made at 850 MHz, 1.7 GHz and 4.0 GHz, rms DS cumulative distributions point out just a little decrease in the rms DS when the frequency increases. In [15], [16] a more consistent rms DS

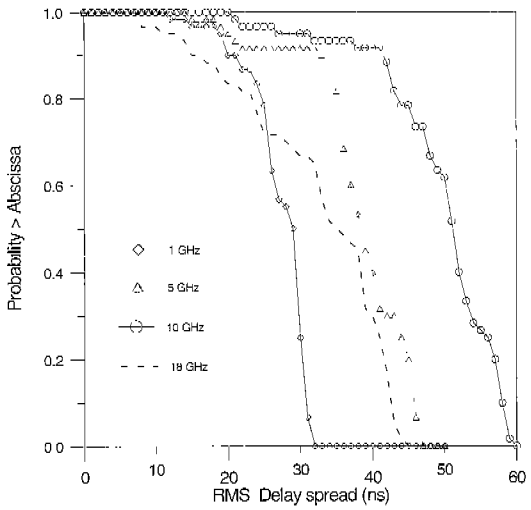

Fig. 7. The cumulative distribution function of the rms DS in the four frequency bands investigated.

reduction with frequency increase was observed. In [26], where measurements at 2.4 GHz, 4.75 GHz, and 11.5 GHz were carried out, the rms DS at 11.5 GHz resulted to be about 30 % smaller than at 2.4 GHz and 4.75 GHz, while no significant changes were observed passing from 2.4 GHz to 4.75 GHz. It has to be remarked that, in the experiment carried out [26], the influence of the antenna gain variations over the frequency band can be neglected as stated by the authors.

In [28] measurements were taken in the frequency domain at 2 GHz, 5 GHz and 17 GHz. The sweep bandwidth was 500 MHz. The CDFs obtained from all measurements show a decrease of mean rms DS with the increase of frequency from 2 GHz to 17 GHz. It has to be noted that, in [28], before measurements were carried out the system was calibrated to compensate for phase and amplitude variations caused by the measurement equipment including the antennas. Transmit and receive antennas adopted in [28] are both bi-conical omnidirectional and, since no more is said about radiation characteristics at 2 GHz, 5 GHz and 17 GHz, it can be supposed that radiation pattern is constant with frequency.

Statistics of the rms DS obtained from the measurements carried out in the present work are shown in Fig. 7. Both LOS and OBS measurements locations (about 60 for each carrier frequency) were used to estimate the CDF.

Rectangular windowing was applied to frequency domain data before processing. Values between 10 ns and 60 ns have been found. This would limit the symbol rate to about 2 Mboud (for BPSK transmission system) in case no channel equalization or multicarrier transmission is applied. Rms DS distributions, obtained in this experiment at different frequencies, can be compared only if antenna influence is taken into account. Fig. 7 results show that, increasing the frequency from 1 GHz to 10 GHz, the CDF curves of rms DS give higher values of the rms Delay Spread for a fixed probability. The observed increase of the rms DS is due to antenna which acts as a spatial filter on the received echoes. This filtering effect quantitatively varies with frequency since the antennas are not scaled versions of each other (they have different antenna radiation pattern and antenna gains). From 1 GHz to 10 GHz discone antennas were

used which, as said in Section II, showed a sensible reduction of the vertical beamwidth with the frequency increase. This fact, as will be explained in section IV using a simple ray-tracing model, caused the observed rms DS increase. At 18 GHz a directive horn antenna at the receiver and a bi-conical antenna at the transmitter were used. The corresponding CDF curve shows, in this case, a different behavior with respect to the other frequencies. In fact, for rms DS values less than 27 ns the probability to exceed the abscissa value is less than the other curves. On the contrary, for higher rms DS values, the probability that the abscissa is exceeded becomes higher than at 1 GHz. This different behavior is explained by observing the experimental rms DS values, shown in Fig. 8, from which the CDFs of Fig. 7 were calculated. These curves compare the rms DS versus the distance (d) when the transmitter is moved along paths L1, L3, L4 of Fig. 4 at 1 GHz, 5 GHz and 18 GHz. It can be noted that when the receiver is in LOS condition the horn antenna improves the channel behavior (lower rms DS). This happens on the overall path L1 and on paths L2 and L3 at a distance less than 4m (first room of Fig. 4).

When the receiver is in OBS condition, the horn antenna (used at 18 GHz) shows worse performance (higher rms DS) than the discone (used at 1 GHz). This is evident in Figs. 8(b) and (c) for $d > 4$m.

For a better understanding of these results, in Fig. 9 two examples of impulse responses in LOS and OBS conditions have been reported. Fig. 9(a) was taken at position L5P3 of Fig. 4 in LOS. It is evident in Fig. 9(a) that many paths which reach the receiver with a relevant amplitude at 1 GHz (omnidirectional antenna) are filtered by the horn antenna at 18 GHz, thus reducing the delay spread. On the contrary, in Fig. 9(b), which corresponds to an OBS position (L3P10), there is a strong path (around 25 ns delay) in the 1 GHz case that is strongly attenuated by the horn antenna at 18 GHz. This path, which could come by a reflection from the right side wall, reaches the receiver with an angle larger than the horn beamwidth in the horizontal plane, so that it is strongly attenuated at 18 GHz. This causes a higher rms DS at 18 GHz.

In Fig. 10 the rms DS cumulative distributions for two values of the transmitting antenna height (1.5m and 2.5m) at 1 GHz and 5 GHz are reported. It can be observed that the rms DS increases when one of the two antennas is raised. A model to explain this result is given in Section IV.

C. Frequency Correlation Function

A significant characterization of frequency selectivity of a transmission channel is obtained through its frequency correlation function. As reported in [11], [12] it is defined as

$$R(k,x) = \frac{1}{N}\sum_{i=1}^{N-k} H^*(f_i,x)H(f_{i-k},x)\,, \qquad k \geq 0\,, \qquad (7)$$

where $H(f_n,x)$ are the measured samples of the channel frequency response. The 3 dB width of $R(k,x)$ magnitude measures the coherence of the channel in the frequency domain, which is inversely proportional to the rms DS of the channel. As an example, in Fig. 11 the impulse responses and the corresponding frequency correlation functions, measured at different

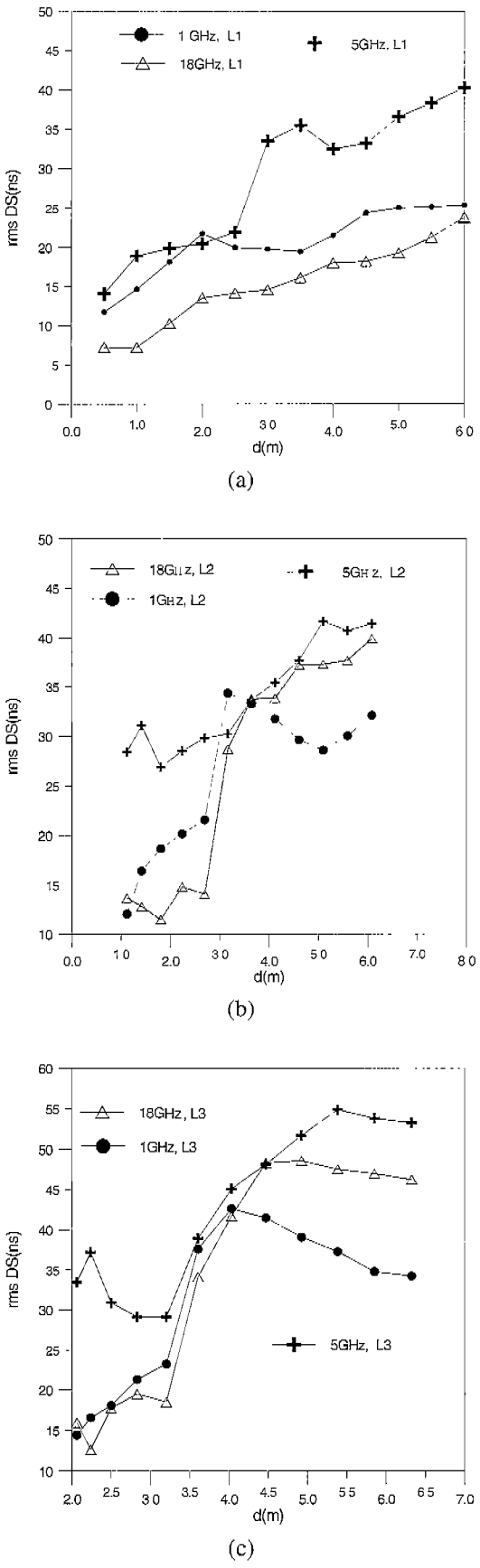

Fig. 8. Experimental values of rms DS versus distance at 1 GHz, 5 GHz and 18 GHz: (a) Path L1, (b) path L2, and (c) path L3.

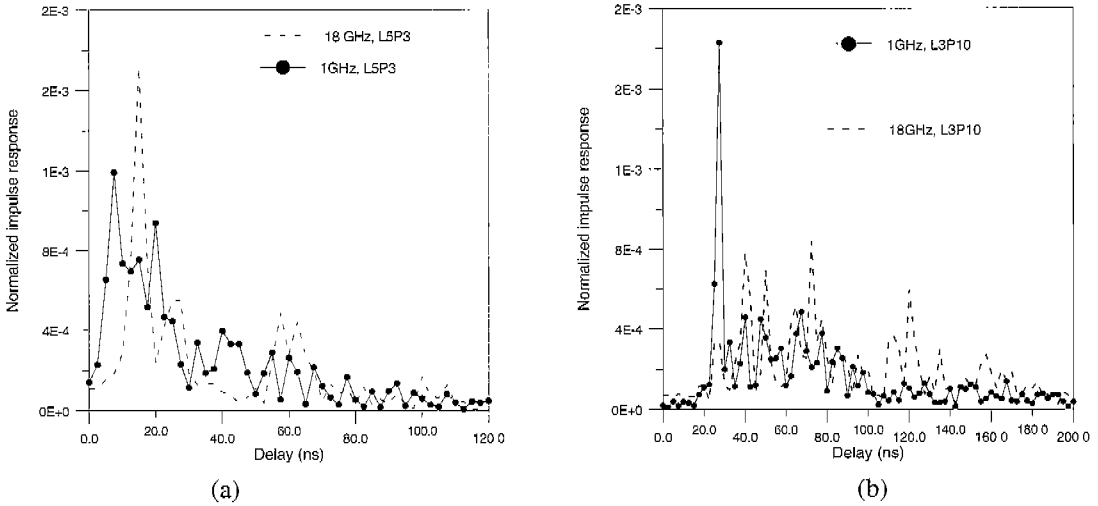

Fig. 9. Normalized measured impulse responses: (a) LOS (position L5P3 of Fig. 4), (b) OBS (position L3P10 of Fig. 4).

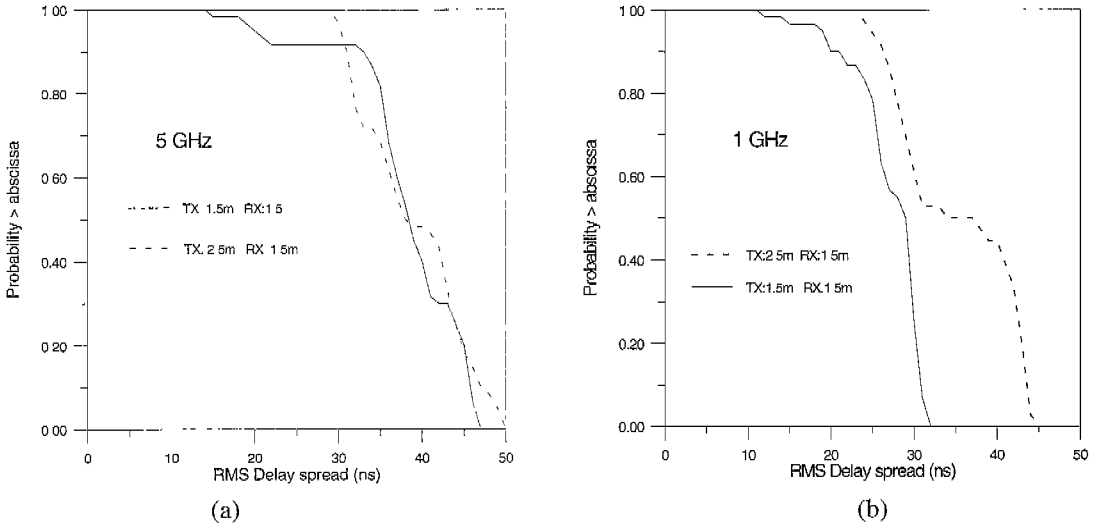

Fig. 10. Comparison between cumulative distributions of rms DS obtained varying the transmitter antenna heights.

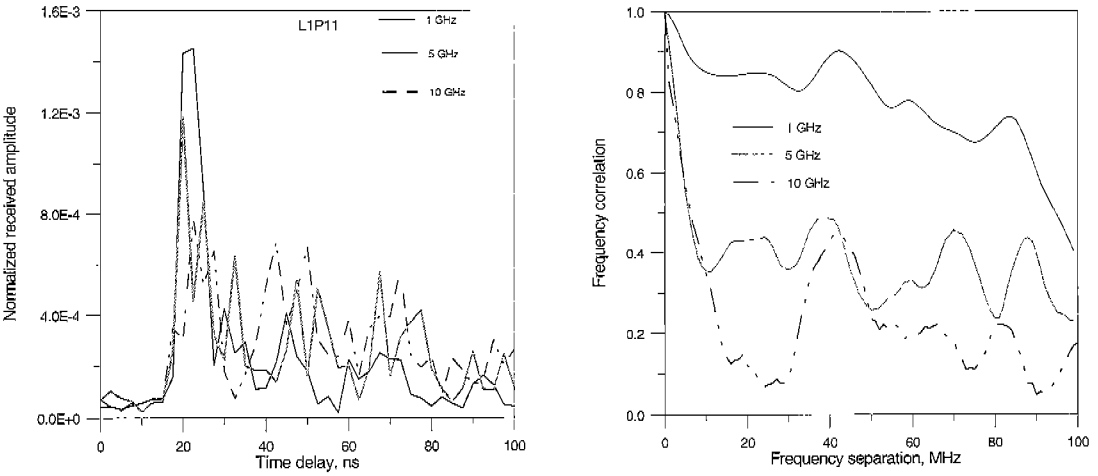

Fig. 11. Comparison between impulsive responses and frequency correlation functions measured at a fixed point at 1 GHz, 5 GHz and 10 GHz.

frequencies in the same measurement point (co-ordinate L1P11 in Fig. 4), are compared. The impulsive response areas have been normalized in order to easily compare them on the same graph. The behavior of these functions confirms that, the measured channel (which includes in our definition the TX-RX antennas) becomes more frequency selective as the frequency in-

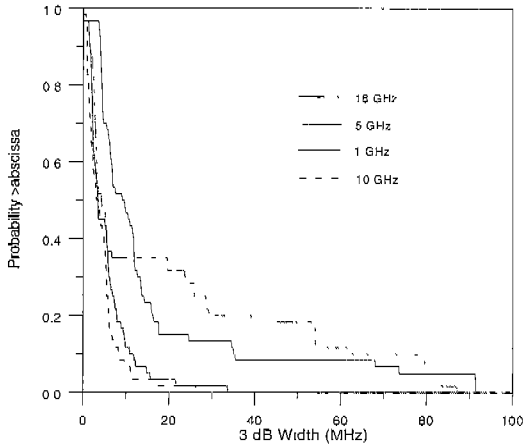

Fig. 12. The CDF of the 3 dB frequency correlation width at 1 GHz, 5 GHz, 10 GHz and 18 GHz.

Table 2. Experimental β values.

Freq.(GHz)/TX height(m)	1	5	10	18
1.5	3.6	2.3	2.5	2.5
2.5	2.28	3	*	*

* not available due to low signal to noise ratio.

creases.

Fig. 11 shows that the frequency correlation function is not a monotonically decreasing function (from frequency separation equal to 0). Thus it seems proper to define the 3 dB width of the frequency correlation function as the frequency distance at which the correlation is for the first time 3 dB lower than the maximum (which occurs at $f = 0$). Fig. 12 shows the CDF of the 3 dB width of the frequency correlation function, B_c , at the four frequencies investigated in this work, with both TX and RX antennas placed at 1.5m height. As for rms DS, both LOS and OBS measurements points were included to estimate these CDFs.

D. Relationship between B_c and rms DS

In this section an attempt to empirically determine a relationship between the 3 dB width(MHz), B_c, of the frequency correlation function and the rms DS(ns) of the channel is made. The model adopted is the following:

$$B_c = C\tau_{rms}^{-\beta}. \tag{8}$$

The constants C and β are determined through a linear regression of the logarithms of (8). Scatter plots of the experimental values of the pairs of parameters $B_c - \tau_{rms}$ are reported in Fig. 13 for all measurements carried out. The MMSE fit is reported on the same graphs on a log-log scale. The values of β can be easily obtained from the fitting equations reported on each figure and are summarized in Table 2. For all experiments, the βs resulted to be in the range between 2.5 and 3.5.

Values of β measured at 1 GHz are reported in [11], [12]. In particular in [11] β varies between 0.66 and 0.91 ($32 < C < 88$) while in [12] β ranges between 1.8 and 2 ($1974 < C < 4113$). It can be observed that values extracted from the measurements carried out in the present experiment are higher. This can be probably attributed to the fact that the measurement environment is quite different (we have mainly metallic walls).

IV. A SIMPLE PROPAGATION MODEL TO EXPLAIN MEASUREMENT RESULTS

In order to better understand the measurement results presented in this paper a simple propagation model was implemented for LOS condition. Neglecting secondary reflections, the power at the receive antenna is given by the sum of the powers of the direct signal, reflections from each of the side walls of the room, reflections from the end walls, a reflection from the ceiling, and a reflection from the floor. In addition, specular reflection is assumed at each wall. The complex envelope of the impulse response of such a channel is

$$h(\tau, r) = \sum_{i=0}^{6} \rho_i a_i(r) e^{-j2\pi f_c \tau_i} \delta(\tau - \tau_i) , \tag{9}$$

where r is the distance between transmitter and receiver, "0" subscript indicates the direct signal, $a_i(r)$ is the amplitude of the ith received echo and is given by

$$a_i(r) = A_0 \frac{\sqrt{G_T(\theta_i, \phi_i) G_R(\theta_i{}', \phi_i{}')}}{r + \Delta\tau_i c} , \tag{10}$$

where A_0 is a coefficient that depends on the transmission parameters (power, frequency, etc.), τ_i represents the propagation delay of the ith signal component, $\Delta\tau_i$ is its delay with respect to that of the direct component (r/c), c is the speed of light, f_c is the carrier (or center) frequency of the corresponding passband channel, ρ_i is the coefficient of reflection pertinent to the path followed by the ith received component, $G_T(\theta_i, \phi_i)$ and $G_R(\theta_i{}', \phi_i{}')$ are the transmit and receiver antenna gain, respectively, corresponding to the direction of emission and reception of the ith signal component. Model (9) has been implemented on a computer and used to evaluate the rms DS in the room shown in Fig. 14.

As an example, in Fig. 15(a) the normalized wideband [Eq. (2) averaged over a 400 MHz bandwidth around the center carrier] and narrowband (only the center carrier is considered) received power versus distance is reported. In this simulation, metallic walls were assumed but reflections from the two side walls were neglected (thus resulting in a 5 paths model). Both transmitter and receiver were at 1.5m height while the ceiling was 3.5m high. Antennas were assumed omnidirectional with eight shaped vertical radiation pattern (the 3dB antenna beamwidth is 80°). The fitted line shows a 1.59 slope that quite well agrees with measured results. The room length was 30m and the distance between TX and its closest end wall was 5m. In Fig. 15(b) the power versus distance relationships are compared when the height of the TX antenna is raised from 1.5m to 2.5m. As shown in this figure the simulation confirms the effect of antenna gain compensation obtained in the measurement results reported in Fig. 5(b) and pointed out in [14].

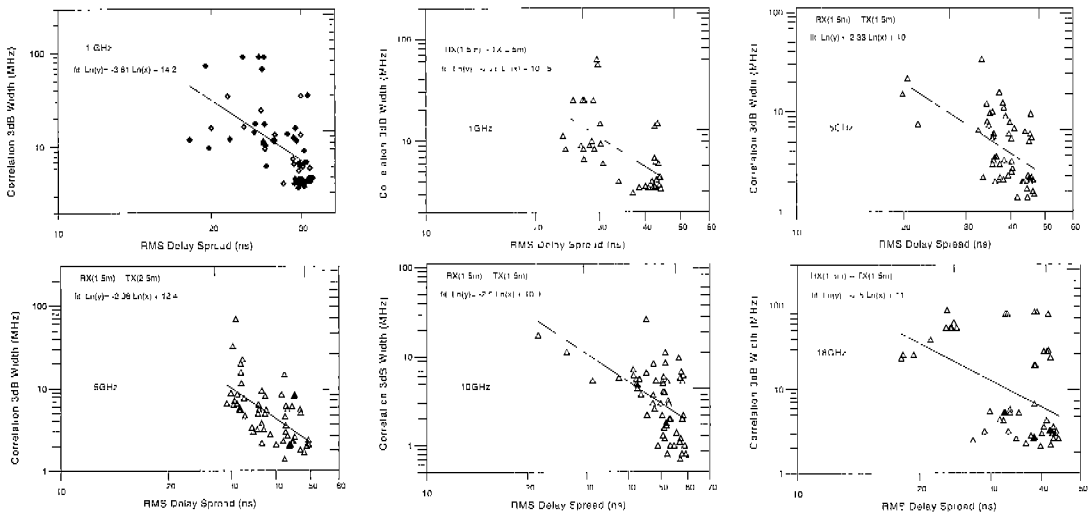

Fig. 13. Scatter plots of the 3 dB width versus the rms DS for all experiments in a log-log scale. Also shown are the lines with the MMSE fit to the data.

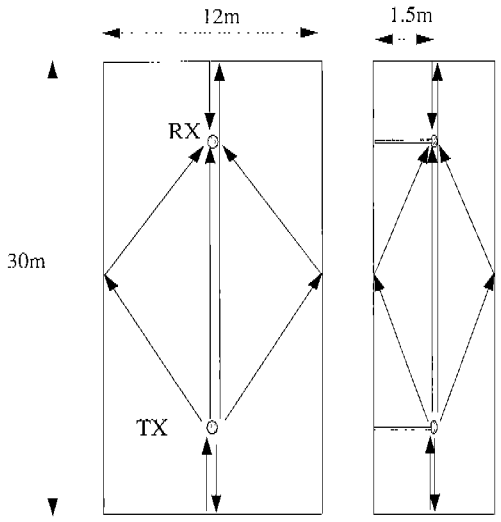

Fig. 14. Plan and elevation drawings showing the seven propagation paths considered in (9).

In order to simulate the variation of rms DS with frequency, the implemented ray tracing program takes into account the dependence of the radiation pattern on frequency. Specifically, the vertical beamwidth is assumed to decrease with frequency while in the horizontal plane the antenna is omnidirectional. In Fig. 16 an example of variation of the vertical radiation pattern with frequency is reported.

An example of variation of the rms DS with distance d between transmitting and receiving antennas and with frequency is reported in Figs. 17(a) and (b). The simulation conditions are the same as those of Fig. 15 but two parameters were separately varied: wall's reflection coefficient and antennas' vertical beamwidth.

In Fig. 17(a), the reflection coefficient is assumed constant while the radiation pattern varies with frequency according to Fig. 16. In Fig. 17(b), the radiation pattern is assumed fixed while the absolute value of the reflection coefficient is increased

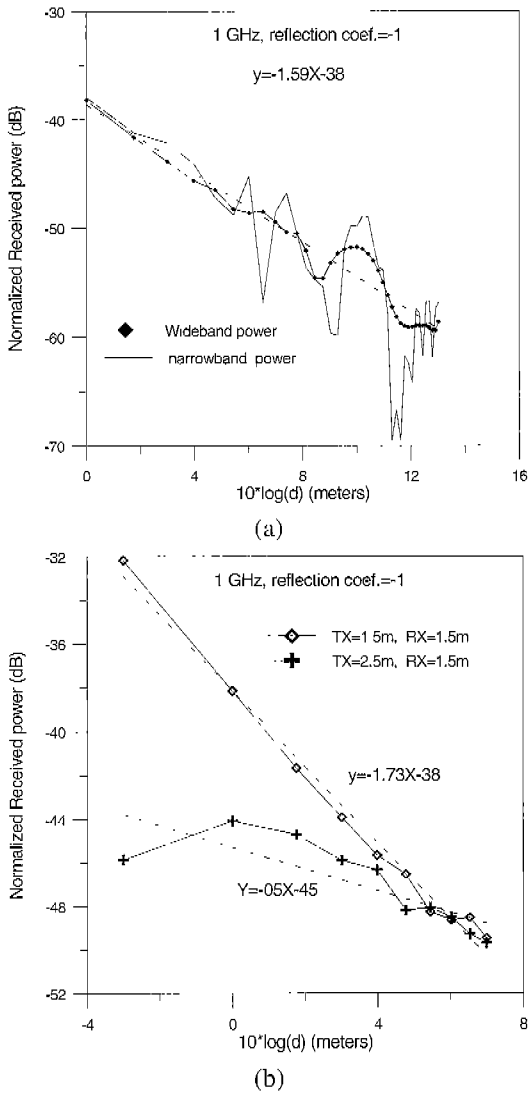

Fig. 15. Simulated wideband normalized received power versus distance with two values of transmitting antenna heights: (a) TX = RX = 1.5m, (b) TX = 2.5m, RX = 1.5m.

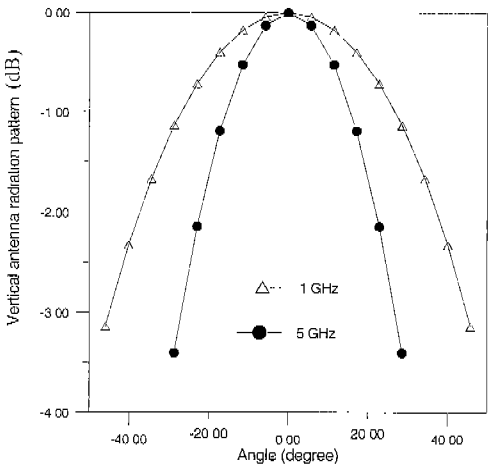

Fig. 16. Model of the variation of the vertical antenna pattern with frequency.

with frequency. In both cases the rms DS increases.

An explanation of the variation of rms DS with distance, shown in Fig. 17, is given in [10].

For the dependence on frequency observed in Fig. 17(a), it has to be considered that if the antenna radiation pattern vertical beamwidth decreases with frequency, the importance of rays which reach the receiver with small angles (and thus large excess delays like for side walls and end walls) is increased with respect to those which experience large angle of arrivals (and thus small excess delays like ceiling and floor reflections). In addition even though reflections from the floor and ceiling have higher amplitudes, they have small excess delays and therefore make only minor contributions to the total rms DS. The contrary happens for side and end-wall contributions which have longer excess delays. Thus, considering the relative paths' contribution to the rms DS, the final effect is that of increasing the rms DS.

As for the dependence of rms DS on reflection coefficients, it must be born in mind that the importance (with respect to the direct path) of all echoes increase with walls' reflectivity thus giving a higher delay spread.

The above reported considerations are confirmed by the two examples of simulated impulse responses at distance respectively of $d = 8$m and $d = 5$m reported in Fig. 18. These graphs have been generated under the same simulation conditions as Figs. 17(a) and (b), respectively. The impulsive responses have been normalized dividing each path amplitude by the square root of the sum of the squares of echo amplitudes. This normalization points out the relative importance of echoes that contribute to the delay spread value. As it can be observed in Fig. 18(a), the amplitude of the first two echoes (from ceiling and floor) is reduced (with respect to the direct path) passing from 1 GHz to 5 GHz, while the contrary happens for the third and fourth paths (two end walls).

In Fig. 18(b) instead, all echo's amplitudes increase with respect to the direct path when the reflection coefficient is higher. Fig. 17 also shows that when the variation of the reflection coefficient with frequency is low, it is mainly the antenna vertical pattern shape which determines the delay spread frequency dependence. To conclude, the simulation confirms that an in-

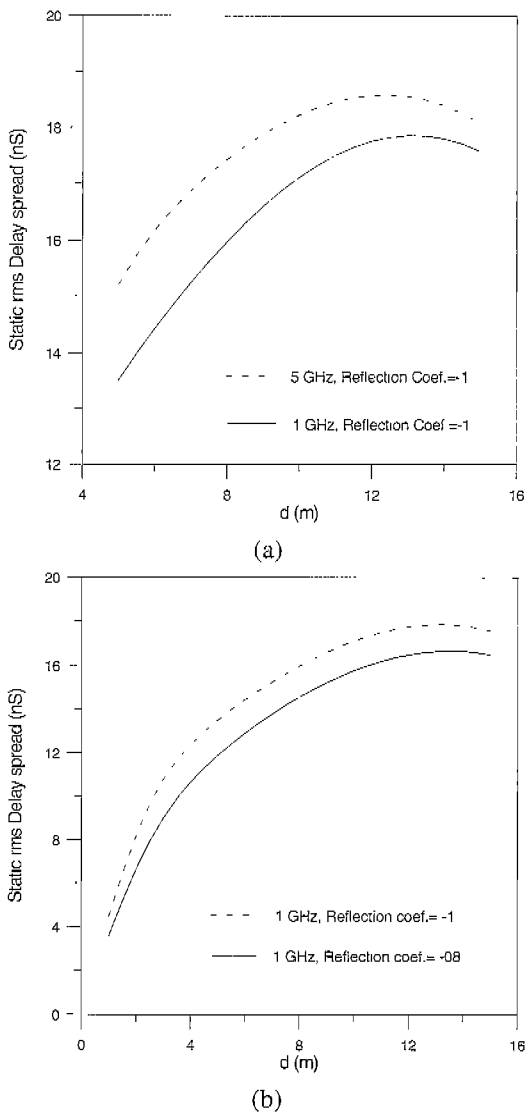

Fig. 17. Static rms DS versus range, computed from simulations for the room geometry shown in Fig. 14: (a) The elevation beamwidth decreases with frequency (constant reflection coefficient), (b) The elevation beamwidth is fixed but the reflection coefficient increases with frequency.

crease of radiation pattern directivity in the vertical plane leads to higher rms DS in the case of the room layout simulated.

In Fig. 19 the dependence of rms DS on the difference in height between transmitting and receiving antennas was simulated. The simulation conditions are the same as those in Fig. 17 but the room length is 40m in order to point out delay spread variations more clearly. As it is shown, when the receiving antenna is raised there is an increase of the delay spread. This simulation result agrees with measurement results shown in Fig. 10 where rms delay spread cumulative distribution is compared at different antenna heights.

The results of Fig. 19 can be interpreted considering that when the receiving height increased, the two antennas are no more aligned along the direction of maximum directivity and this leads to a reduction of received power from the direct path with respect to the reflected ones.

This effect leads to an increase of the rms DS and is partic-

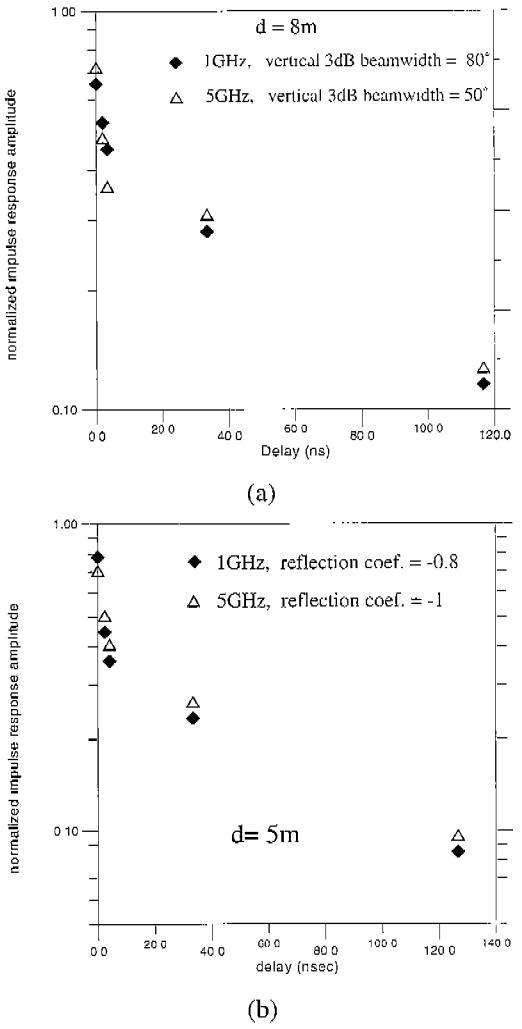

Fig. 18. Simulated channel impulse responses: (a) Effect of variation of the vertical beamwidth, (b) Effect of variation of the reflection coefficient.

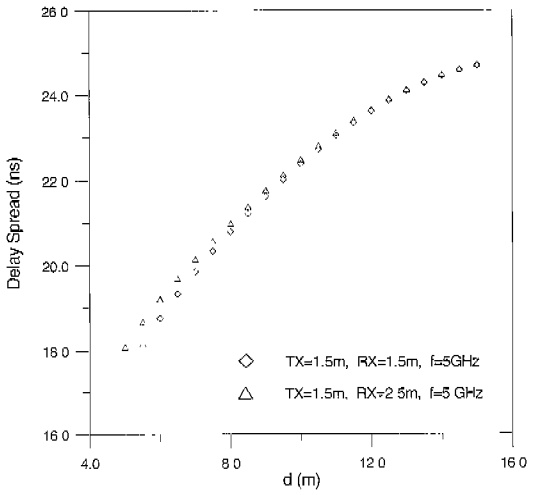

Fig. 19. Variation of rms DS as a function of different heights of transmitting and receiving antennas (ceiling height = 3.5m, room length = 40m, distance of TX from its closest end wall = 10m).

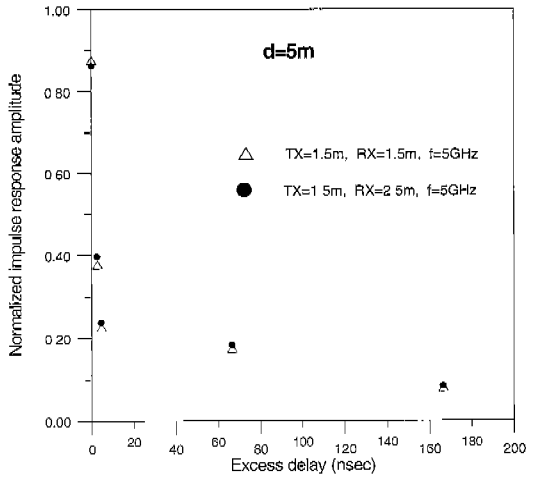

Fig. 20. Examples of normalized impulse responses with two different TX antenna heights.

ularly pronounced when the distance between the antennas is low while it tends to be negligible when it increases. This explains the reduced difference between the two curves of Fig. 19 when the distance increases. In Fig. 20 two examples of impulse response in the same simulation conditions like Fig. 19 at $d = 5$m is reported. As it can be observed, when the TX antenna is raised, all the reflected paths increase their importance with respect to the direct one and this leads to an increase of the rms DS.

V. SUMMARY AND CONCLUSION

Indoor radio propagation measurements at 1 GHz, 5.5 GHz, 10 GHz, 18 GHz, carried out using a network analyzer, are reported. The object of this experiment is to investigate on the influence of antenna pattern on indoor radio channel characteristics. Measurements were performed in an office environment with mainly metallic walls.

From a linear regression of the measured received power values , the exponent of the power-distance relationship is found to be between 1.26 and 1.76 when both TX and RX antennas were at the same height (showing no clear trend versus the frequency) while it approaches to zero when the TX antenna is raised with respect to the receiving one. This latest effect, confirmed by simulation, shows that antenna gain compensation of distance path loss allows to achieve almost uniform coverage throughout a pico-cell as observed in [14]. However the quantitative results highlight the shortcomings inherent in this approach since "uniform coverage" is obtained at the expense of an average higher attenuation throughout the room, thus resulting in a poor coverage. The CDFs of the rms DS have been estimated. The rms DS was found to increase with the frequency at 1 GHz, 5.5 GHz, 10 GHz, where omnidirectional discone antennas were adopted. This effect can be mainly attributed to the variation of the antenna radiation pattern with frequency. The analysis of the simulation, performed in this paper, has confirmed this hypothesis. As an example the rms DS exceeded with probability 0.1 that was 32 ns at 1 GHz, 46 ns at 5 GHz and 58 ns at 10 GHz.

The experiment at 18 GHz, where a directive horn antenna was used at the receiver, showed, with respect to all other frequencies, the lowest rms DS in LOS condition, as expected on the base of intuitive considerations. On the contrary, in OBS

situations the 18 GHz rms DS was higher than at 1 GHz. As an example, the rms DS exceeded for 10 % of time was 42 ns at 18 GHz. This different behavior in OBS and LOS (observed at 18 GHz) can be explained considering the particular configuration of the measurement environment of this experiment and cannot be assumed as a general trend. However, this unexpected result in OBS conditions confirms that indoor propagation is often strictly related to the particular environment and some intuitive considerations may in some cases turn out not to be true.

The effect on the rms DS of varying the relative height between the two antennas has been investigated. An increase of the rms DS was observed when the height of one of the two antennas was increased. This rms DS increase is due to the fact that the two antennas are no longer aligned along the direction of maximum directivity and this leads to a reduction of received power from the direct path with respect to the reflected ones. The CDFs of the 3 dB width of the frequency correlation function have been evaluated.

For example the 3 dB width of the frequency correlation function exceeded with probability 0.9 was in the order of 3 MHz at 5 GHz, 10 GHz, and 18 GHz (with slight differences between them) rising to 5 MHz at 1 GHz. Higher differences have been observed for lower probability values. For example the 3 dB width exceed with probability 0.3 was 25 MHz at 18 GHz, 13 MHz at 1 GHz , 8 MHz at 5 GHz and 6 MHz at 10 GHz.

The empirical relationship between the 3 dB width of the frequency correlation and the inverse of the rms DS was fitted by an exponential function with the exponent ranging from 2.3 to 3.6 at the different the frequencies sounded. The dispersion of the measured points with respect to linear regression resulted to be higher than the results reported in [11] at 1 GHz. To conclude, the increase in rms DS observed in this experiment caused by the reduction of the antenna beamwidth in the vertical plane with frequency increase and/or by the increase of vertical separation between the antennas, demonstrates how antenna design and position strongly impacts transmission performance of wideband indoor systems. Thus, the current trend to move indoor high speed digital communications towards higher frequencies has to be accompanied by a careful design of antennas in order to avoid worsening of the propagation conditions.

APPENDIX A : DISCONE ANTENNAS

The Discone Antenna is intended primarily for vertical polarization and, like a vertical dipole, gives an omnidirectional pattern in the horizontal plane. The discone's most distinctive feature is its simplicity of construction and feeding. Its most important characteristic is satisfactory operation over a wide band of frequencies.

Impedence

A sketch of the discone radiator is shown in Fig. 21 In the following the nomenclature below reported will be used.

ϕ = cone flare angle (total)
L = cone slant height
C_{MAX} = maximum cone diameter
C_{MIN} = minimum cone diameter
D = disk diameter
S = disk-to-cone space

For a fixed value of L, C_{MIN} , ϕ and frequency, the VSWR on a 50 ohm line was measured for various combinations of disk-to-cone spacing S and disk diameter D. A series of such measurements allows a value of S and D to be chosen that gives the best match over the largest range of frequencies. This process was repeated for several values of ϕ . From these data it was determined that the optimum values of S and D/C_{MAX} may be considered to be independent of ϕ, allowing the following simple design formulas to be written

$$S = 0.3\, C_{MIN}$$
$$D = 0.3\, C_{MAX}$$

These relations are independent of L and f; bandwidth is inversely C_{MIN} .

Flare Angle

The slant height is a function of frequency. For all values of flare angle considered, 25 through 90 deg, the slant height is always slightly greater than a quarter-wave length of the lowest frequency at which the antenna is to be operated.

The large-angle discone exhibits some of the characteristics of a high-pass filter in that once the slant height of the cone exceeds approximately $\lambda/4$, the match a 50 ohm line remains good over an extremely wide frequency range. The H-plane pattern of a discone antenna is independent of angle while the E-plane field closely approximates that of a dipole at a frequency near f_0 (here defined as the frequency at which slant height is a fourth wave length). However, as the operating frequency is increased, there is a tendency of the E-plan pattern to push downward, away from the plane containing the disk. Normalized E-plane field patterns for the discone antennas designed for optimum impedence characteristics are shown in Fig. 22 for values of ϕ of 35, 60 and 90 deg. Near f_0 the patterns are nearly independent of flare angle, there being a slight tendency for the pattern to become broader with increased values of ϕ. In this region the patterns are nearly the same as those of a short dipole. At frequencies above approximately $1.5f_0$, the shape of the resulting pattern is affected significantly by the cone flare angle.

Gain Figures

When the transmission frequency is $f = f_0$ the gain figures are like a dipole. Variation of the gain occurs when the ration f/f_0 increases as shown in Fig. 22. For example, the gain in the horizontal plane is approximately 2 dB less than a dipole for the 60 deg discone at $3f_0$, while for the 90 deg discone at $3f_0$, the gain in the horizontal is less than that of a dipole by about 1.5 dB. In the case of a 60 deg antenna the loss in the horizontal plane is 3.3 dB with respect to a dipole at $3.75f_0$.

Implemented Discone Antenna Measurements Results

In Figs. 23 and 24 the measured matching performance of the two discone antennas implemented in the present work are reported. In order to simplify the realization of the discone at 1 GHz it was implemented using tubes(this gives little performance losses).

According to the discone antenna dimensions reported in Fig. 3 it can be obtained that:

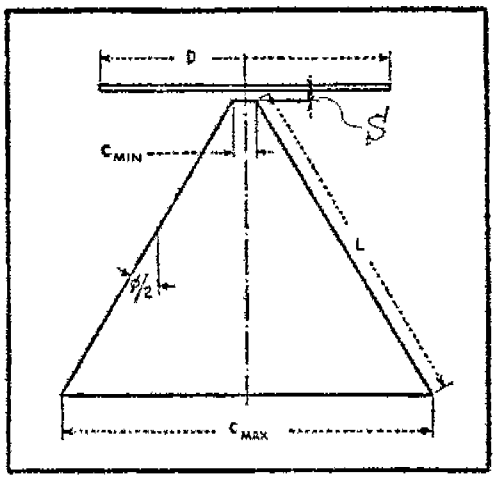

Fig. 21. Discone antenna parameters.

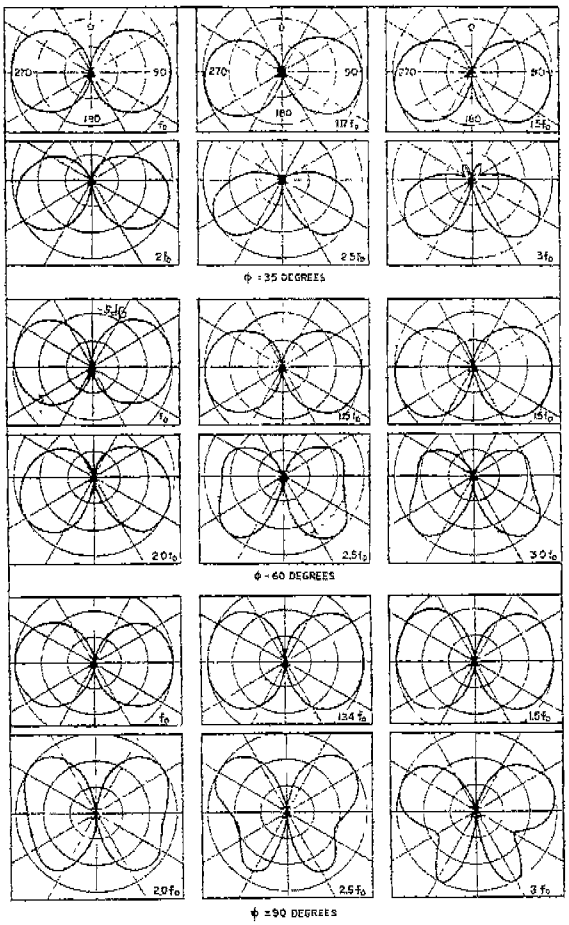

Fig. 22. Relative E-plane normalized field patterns for different angles ϕ.

f_0 = 0.7 GHz when L = 10.7 cm (discone used at 1 GHz), thus f/f_0 = 1.43;

f_0 = 3.75 GHz when L = 2 cm (discone used at 5.5 GHz and 10 GHz), thus f/f_0 = 1.46 at f = 5.5 GHz and f/f_0 = 2.66 at f = 10.0 GHz.

Using f/f_0 obtained values and Fig. 22 it is possible to have an idea of the radiation patterns at f = 1 GHz, 5.5 GHz and 10 GHz.

APPENDIX B : BI-CONICAL ANTENNA

The bi-conical antenna is a waveguide channel of variable section. A feature of the bi-conical antenna is the fact that its electromagnetic field has a spherical wavefront, i.e., the points of identical phase lie of a sphere of constant radius. Other properties are:

- absence of a critical wavelength,
- variable phase velocity,
- transition of the electromagnetic field at enough distance from the antenna into a purely transverse wave (TEM), propagating with the velocity of light.

For the two most important cases (TEM waves excited by a probe and TE_{01}-waves excited by a magnetic dipole parallel to the axes) curves of the gain as a function of the antenna parameters are presented in Figs. 25(a) and (b). In Fig. 25(c) the dependence of the optimum parameters R/λ and D/λ of the bi-conical antenna on the required gain is shown. According to the bi-conical antenna dimensions reported in Fig. 3 it can be obtained that $R = D$ = 9.1 cm, thus D/λ = 5.5 and thus, from Fig. 25, the gain is about 4 dB.

In Fig. 26 the measured matching performance of the implemented bi-conical antenna are reported.

ACKNOWLEDGMENTS

The author gratefully acknowledge the work of Dr. Elio Restuccia for the design and implementation of the antennas. Work carried out in the framework of the agreement between the italian PT administration and the Fondazione Ugo Bordoni.

REFERENCES

[1] T. Ihara, T. Manabe, M. Fujita, T. Matsui, and Y. Sugimoto,"Research activities on millimeter-wave indoor wireless communication systems at CRT," in *Proc. ICUPC'95*, 1995.

[2] T. A. Freeburg, "Enabling technologies for wireless in-building network communications - Four technical challanges, four solutions," *IEEE Commun. Mag.*, Apr. 1991.

[3] G. Yang, K. Pahalavan, and T. J. Holt, "Sector antenna and DFE modems for high speed indoor radio communications," *IEEE Trans. Veh. Technol.*, vol. 43, no. 4, Nov. 1994.

[4] D. M. J. Devasirvatham, "A comparison of time delay spread measurements within two dissimilar office buildings," *IEEE Trans. Antennas Propagat.*, vol. AP-35, pp. 319–324, Mar. 1987.

[5] R. J. C. Bultitude, S. A. Mahmoud, and W. A Sullivan, "A comparison of indoor radio propagation characteristics at 910MHz and 1.75GHz," *IEEE J. Select. Areas Commun.*, vol. SAC-5, pp. 128–137, Feb. 1987.

[6] K. Pahalavan, R. Ganesh, and T. Hotaling, "Multipath propagation measurements on manufacturing floors at 910MHz," *Electron. Lett.*, vol. 3, pp. 225–227, Feb. 1989.

[7] T. S Rappaport and C. D. McGillem, "UHF fading in factories," *IEEE J. Select. Areas Commun.*, vol. 7, pp. 40–48, Jan. 1989.

[8] S. E. Alexander, "Radio propagation within buildings at 900MHz," *Electron. Lett.*, vol. 18, pp. 913–914, Oct. 1982.

[9] H. Hashemi, "Impulse response modeling of indoor radio propagation channels," *IEEE J. Select. Areas Commun.*, vol. 11, no. 7, Sept. 1993.

[10] R. J. C. Bultitude, P. Melancon, H. Zaghloul, G. Morrison, and M. Prokki, "The dependence of indoor radio channel multipath characteristics on transmit/receive ranges," *IEEE J. Select. Areas Commun.*, vol. 11, no. 7, Sept. 1993.

[11] S. J. Howard and K. Pahalavan, "Autoregressive modeling of wide-band indoor radio propagation," *IEEE Trans. Commun.*, vol. 40, no. 9, Sept. 1992.

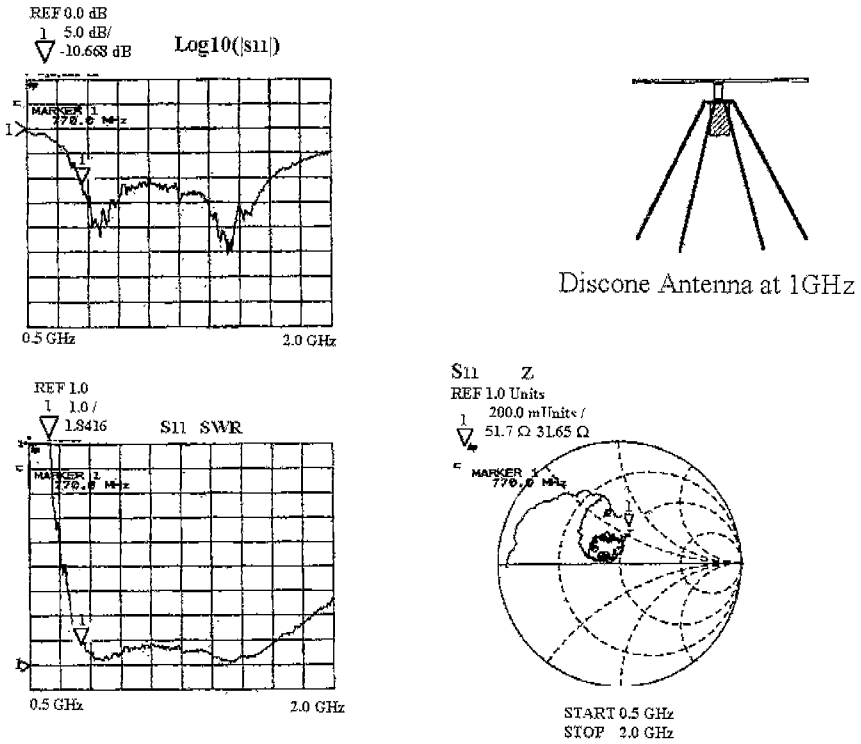

Fig. 23. Matching performance of 1 GHz discone antenna: magnitude of the input reflection coefficient S_{11} versus frequency; voltage standing-wave ratio (VSWR) versus frequency; Smith chart.

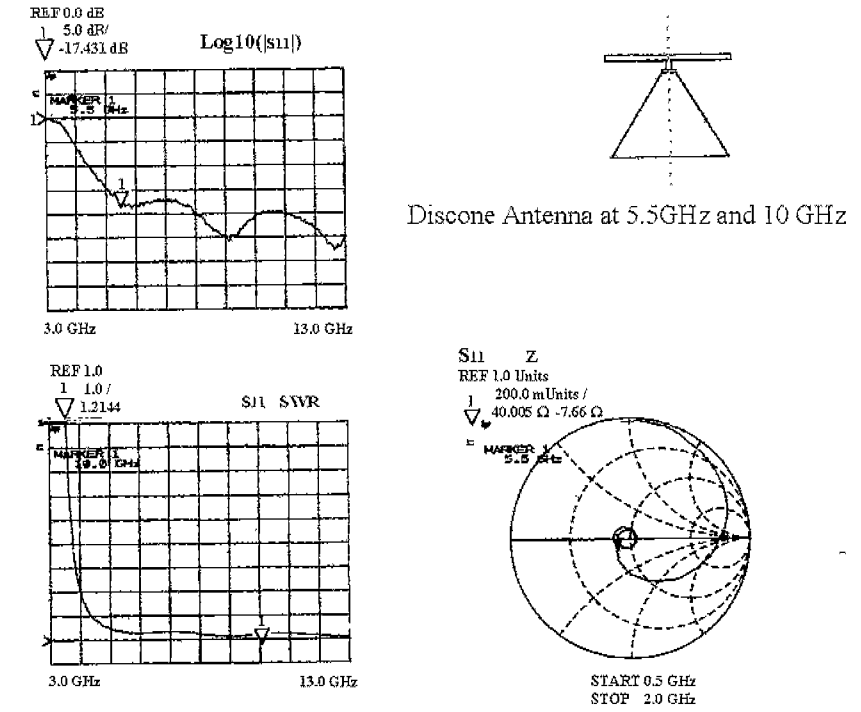

Fig. 24. Matching performance of discone antenna used at 5.5 GHz and 10 GHz: magnitude of the input reflection coefficient S_{11} versus frequency; voltage standing-wave ratio (VSWR) versus frequency; Smith chart.

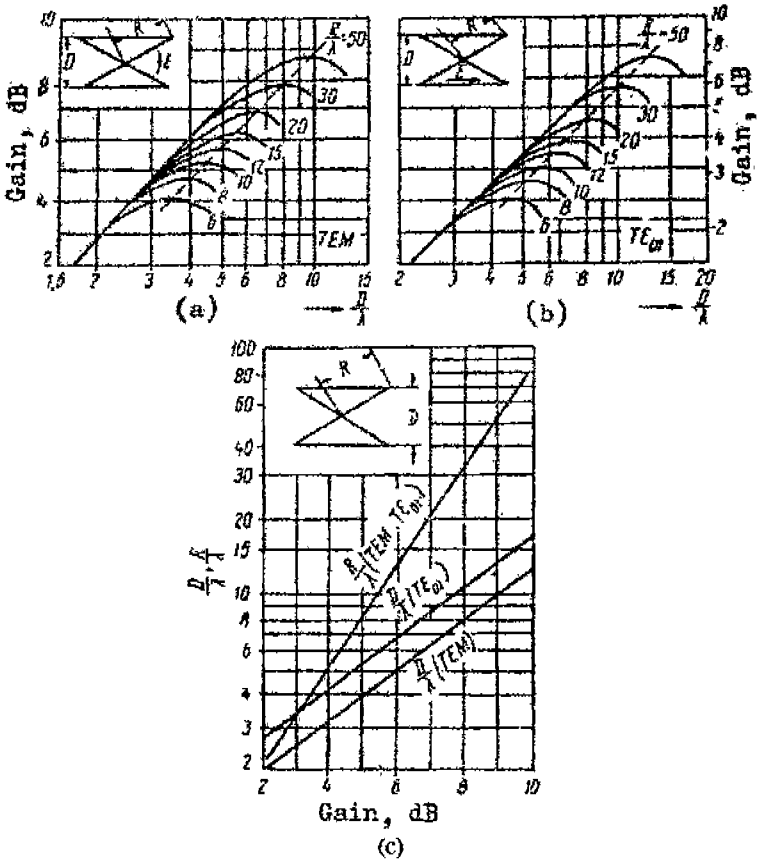

Fig. 25. (a) Graphs of the gain as a function of the parameters of the bi-conical antenna for the TEM wave, (b) The same for the TE_{01} wave, and (c) Graphs of optimum parameters of the bi-conical antenna R and D for required gain.

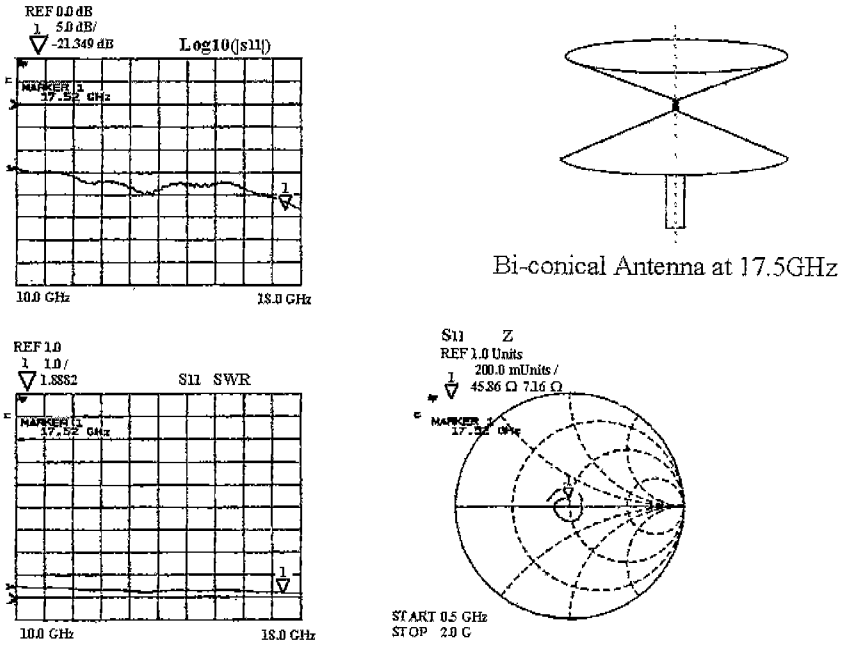

Fig. 26. Matching performance of bi-conical antenna: magnitude of the input reflection coefficient S_{11} versus frequency; voltage standing-wave ratio (VSWR) versus frequency; Smith chart.

[12] S. J. Howard and K. Pahalavan, "Measurement and analysis of the indoor radio channel in the frequency domain," *IEEE Trans. Instr. and Measur.*, vol. 39, no. 5, Oct. 1990.
[13] A. A. M. Saleh, A. J. Rustako Jr., and R. S. Roman, "Distributed antennas for indoor radio communications," *IEEE Trans. Commun.*, vol. COM-35, pp. 1245–1251, Dec. 1987.
[14] P. F. M. Smulders and A. G. Wagemans, "Bi-conical horn antennas for near uniform coverage in indoor areas at mm-wave frequencies," *IEEE Trans. Veh. Technol.*, vol. 43, no. 4, Nov. 1994.
[15] G. J. M. Janssen and R. Prasad, "Propagation measurements in an indoor radio environment at 2.4GHz, 4.75GHz and 11.5GHz," in *Proc. 42th IEEE VTC'92*, May 1992.
[16] P. Nobles, D. Ashworth, and F. Halsall, "Indoor radiowave propagation measurements at frequencies up to 20GHz," in *Proc. 44th IEEE VTC'94*, 1994.
[17] L. W. Pickering, E. N. Barnhart, and M. C. Witten, "Statistical data from frequency domain measurements of indoor PCN communication channel," in *Proc. IEEE PIMRC'91*, King's College, London, Sept. 1991.
[18] P. F. Smulders and A. G. Wagemans, "Frequency domain measurement of the millimeter wave indoor radio channel," *IEEE Trans. Instr. and Measur.*, vol. 44, no. 6, Dec. 1995.
[19] I. Oppermann, J. Graham, and B. S. Vucetic, "Modelling and simulation of an indoor radio channel at 20GHz," in *Proc. IEEE GLOBECOM'95*, 1995.
[20] D. M. J. Devasirvatham, M. J. Krain, and D. A. Rappaport, "Radio propagation measurements at 850 MHz, 1,7GHz and 4GHz inside two dissimilar office buildings," *Electron. Lett.*, vol. 26, no. 7, Mar. 1990.
[21] S. E. Alexander and G. Pugliese, "Cordless communication within buildings: Results of measurements at 600MHz and 60GHz," *Br. Telecom. Tech. J.*, vol. 1, pp. 99–105, July 1983.
[22] A. Z. Fradin, *Microwave Antennas*.
[23] J. J. Nail, "Designing discone antennas," *Electronics*, Aug. 1953.
[24] T. S. Rappaport, *Wireless Communications, Principles and Practice*, IEEE Press, 1996.
[25] G. Santella and E. Restuccia, "Analysis of frequency domain wide-measurements of the indoor radio channel at 1, 5.5, 10 and 18GHz," in *Proc. IEEE GLOBECOM'96*, London, Nov. 1996.
[26] G. J. M. Janssen, P. A. Stigter, and R. Prasad, "Wideband indoor channel measurements and BER analysis of frequency selective multipath channels at 2.4, 4.75, and 11.5GHz," *IEEE Trans. Commun.*, vol. 44, no. 10, Oct. 1996.
[27] C. M. P. Ho, T. S. Rappaport, and M. P. Koushik, "Antenna effects on indoor obstructed wireless channels and a deterministic image-based wideband propagation model for in-building personal communication systems," *Int. J. Wireless Inform. Networks*, vol. 1, no. 1, 1994.
[28] P. Nobles and F. Halsal, "Delay spread and received power measurements within a building at 2GHz, 5GHz and 17GHz," in *Proc. of 10th Int. Conf. Antennas and propagation*, Apr. 1997.

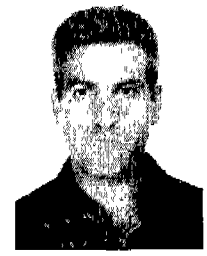

Giovanni Santella was born in Rome, Italy, on June 24, 1961. He received the Electronic Engineering degree from the University of Rome in 1990. Since then he has been working as a researcher in the radio communications area at the Fondazione Ugo Bordoni, in Rome. His research interests cover the characterization and modelling of radio wave propagation in buildings and urban environment and the study and deployment of wideband wireless communication systems. Since 1992 he has performed research on Multicarrier systems. He has been involved in projects supported by the European Community such as RACE-II/dTTb, ACTS-QUOVADIS and ACTS-CABSINET. His current interests are in the areas of spread spectrum systems, mobile communications, and indoor wireless communications.